

Adaptive Soft-Decision Aided Differential Modulation for Cooperative Uplink Transmission Relying on Radio-Over-Fiber Backhaul

Dandan Liang², Varghese Antony Thomas¹, Xinyi Xu¹, Soon Xin Ng¹, Mohammed El-Hajjar¹ and Lajos Hanzo¹

1. Communications, Signal Processing and Control Group, School of ECS, University of Southampton, SO17 1BJ, U.K.
Email: {vat1g10,xx08r,sxn,meh,lh}@ecs.soton.ac.uk

2. Centre for Communications Systems Research, University of Surrey, GU2 7XH , U.K.
Email: d.liang@surrey.ac.uk

Abstract—A novel adaptive turbo-coded soft-decision aided differential detection (ATSDD) scheme is proposed for cooperative uplink wireless and Radio-over-fiber (ROF) transmission in a Fractional Frequency Reuse (FFR) based multicell, multiuser system. More specifically, the ATSDD scheme is employed by the Mobile Station (MS) for reliably conveying the source bits to a pair of Remote Antennas (RAs) by appropriately adjusting the modulation mode according to the near-instantaneous wireless and ROF channel conditions. The ATSDD switching thresholds are specifically adjusted for ensuring that the Bit Error Ratio (BER) remains below 10^{-5} . We also investigated the effect of phase-rotations, which is routinely inflicted by practical imperfect ROF links. We demonstrate that our ATSDD scheme increases the overall throughput.

I. INTRODUCTION

There is an increasing pressure on wireless service providers to satisfy the often conflicting requirements of increased data-rates, improved energy efficiency, better coverage and reduced bandwidth per user. Whilst most of the prior research analysed wireless systems in isolation from the backhaul, the holistic design of the wireless front-end and its backhaul would assist service providers in achieving the above mentioned ambitious targets. Hence this holistic principle has been followed in this paper.

All state-of-the-art wireless systems rely on high-throughput adaptive Quadrature Amplitude Modulation (QAM) [1], [2]. However, their coherent detection requires accurate Channel State Information (CSI). As an attractive design option, the soft-decision based low-complexity M-ary Differential Amplitude and Phase-Shift Keying (M-DAPSK (M_a, M_p)) technique associated with M_a different amplitudes and M_p different phases has been proposed in [3], which outperformed its hard-decision based M-DAPSK counterpart [1], when powerful channel coding schemes [4] are invoked. However, a non-adaptive fixed-throughput scheme would require a high transmit power in order to maintain a low Bit Error Ratio (BER) at the Base Station (BS), even when a powerful channel encoder is utilised for communicating over slowly

The financial support of European Union's Seventh Framework Programme (FP7/2007-2013) under the auspices of the CONCERTO project (grant agreement no 288502) as well as of the RC-UK under the India-UK Advanced technology Centre and that of the European Research Council's Advanced Fellow Grant as well as that of the Royal Society's Wolfson Award is gratefully acknowledged.

fading quasi-static Rayleigh channels. This is due to the lack of temporal diversity within a transmission frame. In contrast to [3] and [5], we propose an adaptive wireless system relying on a low complexity, energy efficient Adaptive Turbo-coded Soft-decision aided Differential Detection (ATSDD) scheme. As a further improvement of the system advocated in [3], Fractional Frequency Reuse (FFR) was invoked in the proposed architecture, which assists in increasing the network's capacity by increasing the frequency re-use factor. Recently, the FFR technique [6] employing multiple Remote Antennas (RAs) has also been adopted in the Long-Term Evolution (LTE) standard [7] for the sake of improving the cell-edge coverage [8], as demonstrated in [5].

However, the FFR scheme of [5] led to a proliferation of the RF components, like oscillators and mixers, which increased the system's cost as well as complexity. Furthermore, the employment of low-cost mixers would lead to a BER degradation in case of high RF frequencies [9]. This is because the architecture of [5] relied on a conventional digital fiber optic communication based backhaul, namely on the Baseband over Fiber (BOF) technique described in [10]. Hence, for the sake of avoiding the above mentioned limitations, in this contribution, we propose an architecture that relies on the efficient Radio Over Fiber (ROF) backhaul, which would ensure that both the cost and complexity of the RAs is reduced in addition to lowering the overall power consumption [11].

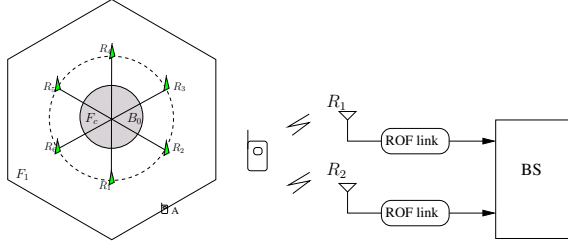
Our novel contributions may be summarised as follows

- 1) FFR based multicell, multiuser schemes operating in a Single-Input Multiple-Output (SIMO) uplink scenario are conceived, when imperfect ROF links are used for connecting a pair of RAs to the BSs.
- 2) Furthermore, a novel adaptive scheme, namely the ATSDD scheme, is designed for the wireless communications link.

The outline of the paper is as follows. Our wireless and ROF system models are illustrated in Sections II and III, respectively, while our results and discussions are presented in Section IV. Finally, our conclusions are offered in Section V.

II. WIRELESS SYSTEM MODEL AND ANALYSIS

Fig. 1(a) presents a hexagonal cell, which is embedded into the 19-cell topology of the FFR based multicell, multiuser



(a) The structure of the central cell and the MS of our proposed uplink adaptive considered locations A, B, C.
 (b) The simplified system block diagram of our proposed wireless-optical SIMO system with ROF link, where \$R_i\$ denotes the \$i\$th RA.

Fig. 1. The schematic of our proposed ATSDD system for wireless-optical communications.

scenario considered [8]. Without loss of generality, the distance between two adjacent BSs is set to \$D = 3\$ km, which corresponds to the Urban-Macro propagation scenario of [8]. Furthermore, the radius of each hexagonal cell is given by \$R_{cell} = D/\sqrt{3}\$ km. The schematic of the ATSDD aided wireless-optical uplink is shown in Fig. 1(b). More specifically, the Mobile Station (MS) transmits the coded symbols \$\mathbf{x}_s\$ to the nearest pair of RAs and communicates over quasi-static Rayleigh fading channels. Then the RAs forward their received signals to the BS without demodulation and decoding. Correspondingly, the \$k\$th symbol received from the \$i\$th RA (\$R_i\$) at the BS may be formulated as:

$$y_{i,k} = A_L e^{j\theta_k} \sqrt{\mathcal{L}_{sr_i}} x_{s,k} h_{sr_i,k} + A_L e^{j\theta_k} n_{sr_i,k} + n_{ri,f}, \quad (1)$$

where \$A_L\$ and \$\theta_k\$ represents the optical fiber's amplitude attenuation, and the phase-rotation introduced by the imperfect optical fiber, respectively, and it will be detailed in Section III. Additionally, \$h_{sr_i,k}\$ denotes the quasi-static Rayleigh fading coefficient, \$\mathcal{L}_{sr_i}\$ denotes the wireless path-loss between the MS and \$R_i\$, and \$n_{sr_i,k}\$ is the noise at \$R_i\$ having a variance of \$N_o/2\$ per dimension, while \$n_{ri,f}\$ is a Gaussian-distributed noise process having a zero mean and a variance of \$N_f/2\$ per dimension, which is used for characterizing the optical link between the RA \$R_i\$ and the BS.

Based on the fixed mode modulation assisted SIMO performance of each of the four half-rate Turbo Coding (TC) aided communication modes recorded for transmission over the combined AWGN and ROF channel, the ATSDD switching thresholds of \$\Gamma = [\gamma_0, \gamma_1, \gamma_2, \gamma_3]\$ may be obtained for the adaptive transmission modes using:

$$\text{Mode} = \begin{cases} \text{NoTx: 0 BPS,} & \text{if } \gamma_r \leq \gamma_0 \\ 4\text{-DPSK: 1 BPS,} & \text{if } \gamma_0 < \gamma_r \leq \gamma_1 \\ 8\text{-DPSK: 1.5 BPS,} & \text{if } \gamma_1 < \gamma_r \leq \gamma_2 \\ 16\text{-DAPSK (2,8): 2 BPS,} & \text{if } \gamma_2 < \gamma_r \leq \gamma_3 \\ 64\text{-DAPSK (4,16): 3 BPS,} & \text{if } \gamma_3 < \gamma_r, \end{cases} \quad (2)$$

where \$\gamma_r\$ is the SNR at the BS's receiver relying on the twin-RN-aided SIMO principle and NoTx denotes the no transmission mode.

At the BS, our soft-decision aided differential detection modem designed in [3] is used, which dispenses with channel estimation for the sake of low-complexity detection. The corresponding Probability Density Function (PDF) of our M-ary Differential Phase Shift Keying (M-DPSK) scheme

receiving \$y_{i,k}\$, when the symbol \$w_k\$ was transmitted may be written as:

$$P(y_k|w_k) \approx e^{-\frac{|y_k - y_{k-1} w_k|^2}{N_f + |A_L|^2 N_0}}. \quad (3)$$

When considering 64-DAPSK (4,16) as an example, the PDF of receiving an \$M_p\$-PSK symbol \$w_k\$ conditioned on the amplitude-selection bits \$b_5 b_4\$ being transmitted may be formulated as [3]:

$$\begin{aligned} P(y_k|w_k, b_5 b_4 = 00) &\approx e^{-\frac{|y_k - y_{k-1} \alpha^0 w_k|^2}{N_0^{(0)}}}, \\ P(y_k|w_k, b_5 b_4 = 01) &\approx e^{-\frac{|y_k - y_{k-1} \alpha^{-3} w_k|^2}{N_0^{(-3)}}} + e^{-\frac{|y_k - y_{k-1} \alpha^1 w_k|^2}{N_0^{(1)}}}, \\ P(y_k|w_k, b_5 b_4 = 10) &\approx e^{-\frac{|y_k - y_{k-1} \alpha^{-2} w_k|^2}{N_0^{(-2)}}} + e^{-\frac{|y_k - y_{k-1} \alpha^2 w_k|^2}{N_0^{(2)}}}, \\ P(y_k|w_k, b_5 b_4 = 11) &\approx e^{-\frac{|y_k - y_{k-1} \alpha^{-1} w_k|^2}{N_0^{(-1)}}} + e^{-\frac{|y_k - y_{k-1} \alpha^3 w_k|^2}{N_0^{(3)}}}, \end{aligned}$$

where the amplitude ratio of the 64-DAPSK constellation rings is \$\alpha^{q_k} = \frac{a_k}{a_{k-1}}\$ with \$a_k\$ and \$a_{k-1}\$ denoting the \$k\$th and \$(k-1)\$st amplitude value, while \$q_k\$ obeys \$(1 - M_a) \leq q_k \leq (M_a - 1)\$. The effective noise variance related to the noise \$n_{sr_i,k}\$ at the RA \$R_i\$ and at the BS, depends on the amplitude ratio \$\alpha^{q_k}\$ used during the \$k\$th symbol instant, which may be estimated as:

$$N_0^{q_k} = N_f + |\alpha^{q_k}|^2 |A_L|^2 N_0, \quad (4)$$

where the noise \$n_f\$ at the BS represents the AWGN having a variance of \$N_f/2\$ per dimension. Furthermore, the PDF of the received signal conditioned on the amplitude-selection bits determined for the SIMO scenario may be expressed as:

$$\begin{aligned} P(y_{1,k}, y_{2,k}|w_k, b_5 b_4) &= P(y_{1,k}|w_k, b_5 b_4) \times P(y_{2,k}|w_k, b_5 b_4). \end{aligned} \quad (5)$$

III. RADIO OVER FIBER MODEL

Fig. 2(a) shows the block diagram of a typical ROF uplink, which consists of an optical modulator at the RA, the optical fiber and finally the photo-detector along with an electronic filter employed at the BS. The electronic RF signal \$V_{RF}(t)\$ at \$f_{RF} = \frac{\omega_{RF}}{2\pi}\$ Hz, that is received at the RA, is modulated onto the optical carrier by the optical modulator, followed by the transmission of the optical signal to the BS, where it is photo-detected and filtered in order to generate the signal \$\hat{V}_{RF}(t)\$. These components are discussed in the following sections. The employment of a ROF link results in a simple RA implementation, while centralised signal processing is used at the BS, including down-conversion, demodulation and detection. Thus, the overall system's cost is reduced, since the hardware can be shared at the base station. The presence of centralised signal processing also facilitates convenient system upgrades.

A. Optical Modulation

The output optical field \$E_{laser}(t)\$ of the laser diode (LD) of Fig. 2(a) operating at a frequency of \$f_c = \frac{\omega_c}{2\pi}\$ Hz and at a power of \$P_{laser}\$ is expressed as follows [12]:

$$E_{laser}(t) = \sqrt{2P_{laser}} e^{j\omega_c t}. \quad (6)$$

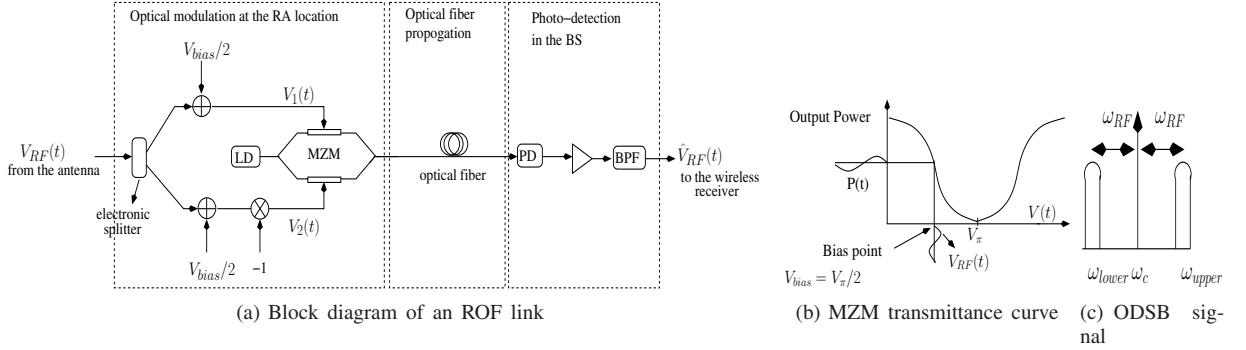


Fig. 2. Details of the ROF link

The output of the laser is fed to the optical modulator, which in this case is a dual-drive Mach-Zehnder Modulator (MZM), where the MZM is biased to a voltage of V_{bias} and driven by the RF signal $V_{RF}(t)$, as shown in Fig. 2(a). Thus, the total applied voltage is $V(t) = V_{bias} + V_{RF}(t)$, where $V(t)$ is applied differentially to the two arms, using the voltages of $V_1(t)$ and $V_2(t)$, i.e. we have $V(t) = V_1(t) - V_2(t)$. Mathematically, $V_1(t)$ and $V_2(t)$ are as follows:

$$V_1(t) = -V_2(t) = \frac{V(t)}{2} = V_{bias}/2 + V_{RF}(t)/2. \quad (7)$$

The arms of the MZM modulator are made from materials like Lithium Niobate ($LiNbO_3$), whose refractive index varies as a function of the voltage applied to them thereby resulting in phase modulation of the signal in each arm. Thus, the output optical field $E_{MZM}(t)$ and the intensity $P_{MZM}(t)$ of the dual-drive MZM, having an insertion loss of t_{attn} dB, can be mathematically expressed as follows:

$$\begin{aligned} P_{MZM}(t) &= |E_{MZM}(t)|^2 \\ &= \left| \frac{E_{laser}(t)\sqrt{t_{attn}}}{2} \left[e^{j\pi \frac{V_1(t)}{V_\pi}} + \gamma e^{j\pi \frac{V_2(t)}{V_\pi}} \right] \right|^2, \\ &= \frac{P_{laser}t_{attn}}{2} [1 + \gamma^2 + 2\gamma \cos(\frac{\pi(V_1(t) - V_2(t))}{V_\pi})] \\ &= \frac{P_{laser}t_{attn}}{2} [1 + \gamma^2 + 2\gamma \cos(\frac{\pi(V_{bias} + V_{RF}(t))}{V_\pi})], \end{aligned} \quad (8)$$

where V_π is the switching voltage of the MZM and $\gamma = (\sqrt{\epsilon} - 1)/(\sqrt{\epsilon} + 1) \approx 1$. Here the switching voltage is the voltage required for imposing a phase change of π radians on a signal propagating in each of the MZM's arms, while ϵ is the MZM extinction ratio, which is defined as the ratio of the maximum to the minimum optical power output of the MZM. Thus, the MZM modulates the intensity of the optical signal according to the modulating RF signal. Fig. 2(b) illustrates the output optical power versus $V(t)$ transmittance curve of the MZM for the ideal case of infinite extinction ratio. As shown in Fig. 2(b), using a bias voltage of $V_{bias} = V_\pi/2$ generates the Optical Double Sideband (ODSB) signal of Fig. 2(c), where the carrier-sideband separation is ω_{RF} .

B. Optical Fiber

Following MZM assisted modulation, the signal is transmitted through an optical fiber from the RA to the BS, as shown in Fig. 2(a). The modulated optical signal propagation through the single-mode optical fiber is characterized by the

following Non-Linear Schrödinger (NLS) equation [8], [13]:

$$\frac{\partial A(z, T)}{\partial z} = -\frac{\alpha}{2} A(z, T) - i \frac{\beta_2}{2} \frac{\partial^2 A(z, T)}{\partial T^2} + i\gamma |A(z, T)|^2 A(z, T), \quad (9)$$

where $A(z, T)$ is the envelope of the modulated optical carrier after propagation through z meters of the fiber, α is the fiber attenuation parameter, γ is the fiber non-linearity parameter and $T = t - \frac{z}{v_g}$ is the time-axis that is moving at the propagation velocity v_g of the envelope $A(z, T)$. Furthermore, we have $\beta_2 = -D \frac{2\pi c}{\omega_c^2}$, where D is the fiber dispersion parameter [13].

Fiber attenuation occurs both owing to the Rayleigh scattering of light in the fiber as well as due to material absorption, where the optical power $P(z)$ after propagation through z meters of fiber may be expressed as follows [13]:

$$P(z) = P_{laser} e^{-\alpha z}. \quad (10)$$

On the other hand, the fiber-induced dispersion is due to the fact that the fiber's refractive index $n(\omega)$ is different for the different frequencies within the bandwidth of the modulated optical signal. The velocity of the optical wave propagation is $v_p(\omega) = c/n(\omega)$ and it is this dependence of the propagation velocity on the optical frequency that results in fiber dispersion [13]. Dispersion results in the attenuation of the photo-detected signal power, which is proportional to $\cos^2 \left[\frac{\pi \cdot L \cdot D \cdot \omega_c^2 \cdot f_{RF}^2}{c} \right]$ [14].

Finally, the dependence of the fiber's refractive index on the propagating optical power contributes to its non-linear behaviour [13], where the varying levels of the instantaneous power result in a time-varying refractive index, which in turn modulates the phase of the propagating optical signal characterized in Fig. 2(a). This phenomenon is typically referred to as Self-Phase Modulation (SPM).

We assume that the links spanning from the RAs to the BS B_0 obey the structure of Fig. 1(a) and Fig. 1(b), which are constituted by realistic, rather than perfect optical fiber links. The simulation of the NLS equation based fiber propagation was carried out using the Split Step Fourier Transform (SSFT) technique of [5], [13].

Furthermore, we explore the robustness of the proposed ATSD scheme to any phase-rotations imposed by the imperfect ROF link, where a model for the phase-rotation imposed by an imperfect optical fiber based link has been proposed in [5]. Specifically, the phase of the k th transmitted

signal may be modelled by:

$$\theta_k = \theta_{k-1} + \tilde{\delta}, \quad (11)$$

where $\tilde{\delta}$ is the phase difference between the k th and the $(k-1)$ st transmitted signal. In Equation (11), $\tilde{\delta}$ varies randomly and may take any value in the range $\{-\delta, \delta\}$ with equal probability. In Section IV, we will analyse the performance of our proposed ATSDD system, where the maximum tolerable value of δ for the various wireless modes will be presented.

Furthermore, Table I shows the parameters of the analogue ROF link used in our paper. Again, the pair of RAs seen in Fig. 1 support the MS's uplink transmission with the aid of a SIMO structure [4] connected to the BS using realistic imperfect optical fiber.

TABLE I
SIMULATION PARAMETERS FOR THE ROF LINK.

Centre Frequency	1.95 GHz
Optical wavelength λ_c	1550 nm
Transmit Power P_{laser}	-6.55 dBm
MZM Extinction Ratio ϵ	15 dB
MZM Insertion Loss t_{attn}	4 dB
MZM Switching Voltage V_π	6 volt
Fiber Length L	4.33 km
Fiber Attenuation Parameter α	0.2 dB/km
Fiber Non-linearity γ	2 /W/km
Dispersion Parameter D [13]	15.68 ps/(km · nm)
Photo-receiver Amplifier Noise Figure	6 dB

C. Photo-detection

After propagation through the fiber, the received signal is optical-to-electronic converted using the photo-detector of Fig. 2(a). If $E_{received}(t)$ is the optical field after fiber propagation, then the photo-diode generates a current $I(t)$ that is proportional to the optical intensity, i.e. $I(t) = R|E_{received}(t)|^2 + n(t)$ [13]. Here, $n(t)$ is the noise of the ROF link, including the laser intensity noise, the shot noise, dark current noise and thermal noise [13]. The photo-detected signal contains the transmitted RF signal, since this signal had modulated the intensity of the optical carrier during optical modulation. This received RF signal is amplified and then filtered using a Band Pass Filter (BPF) centered at f_{RF} Hz.

IV. SIMULATION RESULTS

The performance of our ATSDD scheme proposed for the uplink of the wireless-optical scheme of Fig. 1 is characterized in Fig. 3 using the simulation parameters of Table II.

Firstly, the BER versus SNR performance of the fixed mode based soft-decision aided differential detection is considered in Fig. 3(a), when phase-rotations denoted by δ are imposed by the imperfect ROF link, while assuming that the CSI of the wireless link and the phase-rotations inflicted by the optical-fiber link are both unknown. Observe in Fig. 3(a), that δ imposes different effects on different modes. More specifically, the TC-4DAPK scheme breaks down at a phase-rotation of $\delta = 1.4$ radian (252°), while the TC-64DAPK becomes dysfunctional at $\delta = 0.6$ radian (108°). Based on the performance seen in Fig. 3(a), a phase rotation of upto $\delta = 0.4$ radian (72°) will be imposed in the subsequent simulations

TABLE II
SIMULATION PARAMETERS OF THE WIRELESS LINK.

Coding Modulation	TC
Modulation Scheme	4-DPSK, 8-DPSK, 16-DAPSK (2,8), 64-DAPSK (4,16)
Mapper type	Gray-labelled
Number of iterations	4 inner, 2 outer
Code Rate	1/2
Code Memory	3
Decoder type	Approximate Log-MAP
Symbols per frame	1,200
Number of frames	10,000
Channel	AWGN, Quasi-static Rayleigh fading channel, Optical channel

of our proposed ATSDD scheme. The corresponding modem-mode switching levels are $\Gamma = [5.37, 8.35, 12.75, 18.88] \text{ dB}$, when aiming for a BER of 10^{-5} .

The mode selection probability of each transmission mode recorded, when communicating over a quasi-static Rayleigh fading wireless channel and a ROF channel, is presented in Fig. 3(b). Observe in Fig. 3(b) that when the channel quality is poor, the NoTx mode is employed more frequently, while the 64-DAPSK (4,16) mode is used more often, when the SNR increases. The BER and BPS performance curves of our adaptive system are shown in Fig. 3(c), where we observe that the overall BER was indeed lower than the target BER of 10^{-5} , while the BPS throughput curve improves, as the SNR increases.

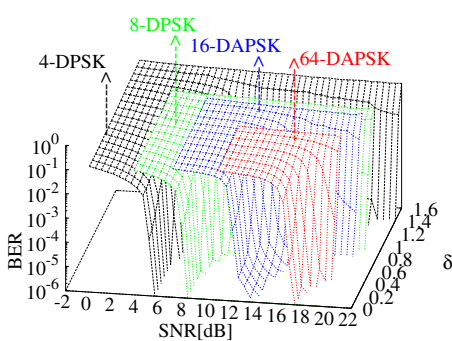
Finally, Fig. 3(d) depicts the 3D throughput of the ATSDD scheme for the entire cellular area of Fig. 1(a) at SNR = 7 dB. The six distinctive throughput peaks correspond to the six locations of the RAs and indicate that a higher throughput may be obtained, when the MS is closer to the RAs.

V. CONCLUSIONS

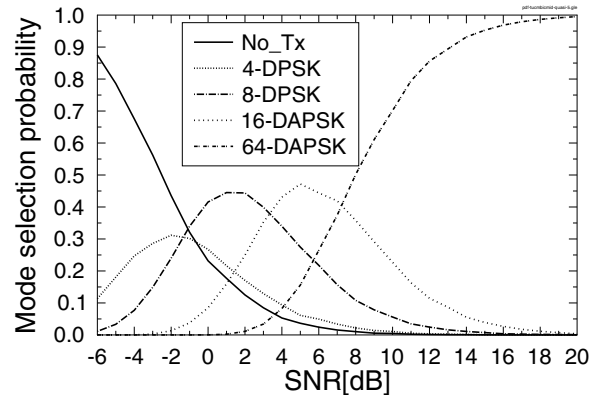
In this contribution, we have proposed an ATSDD scheme for ROF aided and RA-assisted uplink transmission in a FFR based multicell, multiuser system. A combination of the wireless and imperfect optical-fiber channels was considered, which imposed different imperfections. We have demonstrated that our proposed ATSDD scheme constitutes a practical, low complexity, energy efficient design. More specifically, our proposed ATSDD scheme has six regions of high throughput, compared to the flat throughput characteristics of the fixed TC-4DPSK scheme at SNR of 7dB.

REFERENCES

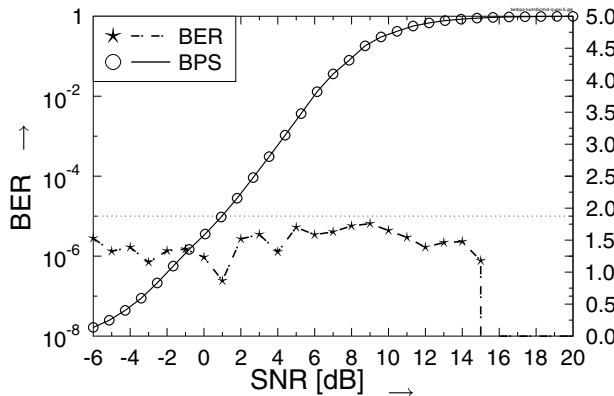
- [1] L. Hanzo, S. X. Ng, T. Keller, and W. Webb, *Quadrature Amplitude Modulation: From Basics to Adaptive Trellis-Coded, Turbo-EQUALISED and Space-Time Coded OFDM, CDMA and MC-CDMA Systems Digital Communications*, 2nd ed. Wiley-IEEE Press, 2004.
- [2] L. Chen, H. Kusaka, and M. Kominami, "Blind phase recovery in QAM communication systems using higher order statistics," *Signal Processing Letters, IEEE*, vol. 3, no. 5, pp. 147 –149, May. 1996.
- [3] D. Liang, S. X. Ng, and L. Hanzo, "Near-capacity turbo coded soft-decision aided DAPSK/Star-QAM for amplify-and-forward based cooperative communications," *IEEE Transactions on Communications*, vol. 61, no. 3, pp. 1080–1087, 2013.
- [4] L. Hanzo, M. El-Hajjar, and O. Alamri, "Near-capacity wireless transceivers and cooperative communications in the MIMO era: evolution of standards, waveform design, and future perspectives," *Proceedings of the IEEE*, vol. 99, no. 8, pp. 1343–1385, August 2011.



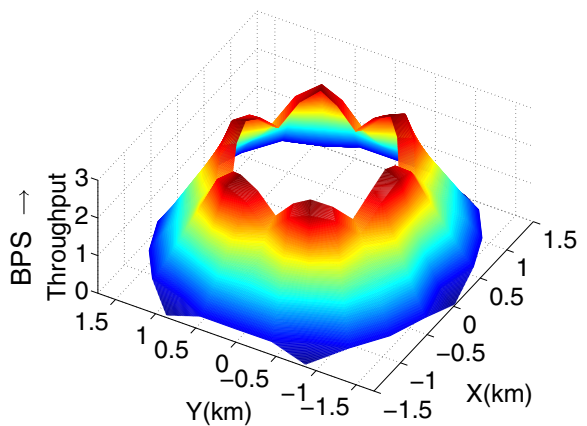
(a) BER versus SNR versus δ performance of the ATSDD schemes of Fig. 1(a) and Fig. 1(b) for transmission over AWGN and imperfect optical channels. The corresponding simulation parameters are summarised in Table II.



(b) The selection probability of each differential modes chosen when transmitting over quasi-static Rayleigh fading and ROF optical channels when the MS locates 'A' (in Fig. 1(a)). A phase rotation of upto $\delta = 0.4$ radian (72°) is considered in the optical link.



(c) The BER, BPS of 4-DPSK, 8-DPSK, 16-DAPS and 64-DAPS for TC transmissions over quasi-static Rayleigh fading and imperfect optical channels when the MS locates 'A' (in Fig. 1(a)). A phase rotation of upto $\delta = 0.4$ radian is considered in the optical link. The relative simulation parameters are detailed in Table II.



(d) The 3D throughput for the ATSDD scheme of Fig. 1(a) for transmission over quasi-static Rayleigh fading wireless and imperfect optical channels for the whole cell with SNR = 7 dB. A phase rotation of upto $\delta = 0.4$ radian is considered in the optical link. The other simulation parameters are summarised in Table II.

Fig. 3. Simulations results for our proposed ATSDD system for wireless and imperfect optical channels.

- [5] D. Liang, X. Xu, S. X. Ng, and L. Hanzo, "Turbo-coded Star-QAM for cooperative wireless and optical-fiber communications," in *IEEE 3rd International Conference on Photonics, Kuala-Lampur, Malaysia*, Oct. 2012, pp. 267 -271.
- [6] H. Huh, H. C. Papadopoulos, and G. Caire, "Multiuser MISO Transmitter Optimization for Intercell Interference Mitigation," *IEEE Transactions on Signal Processing*, vol. 58, no. 8, pp. 4272-4285, 2010.
- [7] H. Ekstrom, A. Furuskar, J. Karlsson, M. Meyer, S. Parkvall, J. Torsner, and M. Wahlgqvist, "Technical solutions for the 3G long-term evolution," *IEEE Communications Magazine*, vol. 44, pp. 38- 45, 2006.
- [8] X. Xu, R. Zhang, S. Ghafoor, and L. Hanzo, "Imperfect digital-fiber-optic-link-based cooperative distributed antennas with fractional frequency reuse in multicell multiuser networks," *IEEE Transactions on Vehicular Technology*,, vol. 60, no. 9, pp. 4439 -4449, Nov. 2011.
- [9] G. H. Nguyen, B. Cabon, and Y. Le Guennec, "Generation of 60-GHz MB-OFDM signal-over-fiber by up-conversion using cascaded external modulators," *IEEE/OSA Journal of Lightwave Technology*, vol. 27, no. 11, pp. 1496-1502, June 2009.
- [10] C. Lim, A. Nirmalathas, Y. Yang, D. Novak, and R. Waterhouse, "Radio-over-fiber systems," in *Communications and Photonics Conference and Exhibition (ACP), 2009 Asia*, vol. 2009-
- Supplement, 2009, pp. 1-10.
- [11] Y. Yang, C. Lim, and A. Nirmalathas, "Comparison of energy consumption of integrated optical-wireless access networks," in *Optical Fiber Communication Conference and Exposition (OFC/NFOEC), 2011 and the National Fiber Optic Engineers Conference*, 2011, pp. 1-3.
- [12] J. Corral, J. Marti, and J. Fuster, "General expressions for IM/DD dispersive analog optical links with external modulation or optical up-conversion in a Mach-Zehnder electrooptical modulator," *IEEE Transactions on Microwave Theory and Techniques*, vol. 49, no. 10, pp. 1968-1976, Oct 2001.
- [13] G. P. Agrawal, *Nonlinear fiber optics*, 4th ed. Academic Press, 2006.
- [14] G. Smith and D. Novak, "Broad-band millimeter-wave (38 GHz) fiber-wireless transmission system using electrical and optical SSB modulation to overcome dispersion effects," *Photonics Technology Letters, IEEE*, vol. 10, no. 1, pp. 141 -143, jan. 1998.